Journal of Photochemistry and Photobiology A: Chemistry 244 (2012) 9–17

Contents lists available at SciVerse ScienceDirect

Journal of Photochemistry and Photobiology A: Chemistry

journal homepage: www.elsevier.com/locate/jphotochem

Fluorescence behavior of ethidium bromide in homogeneous solvents and in presence of bile acid hosts

Smritakshi Phukan, Sivaprasad Mitra*

Department of Chemistry, North-Eastern Hill University, Shillong 793 022, India

ARTICLE INFO

Article history:
Received 17 April 2012
Received in revised form 18 June 2012
Accepted 25 June 2012
Available online 2 July 2012

Keywords:
Fluorescence solvatochromism
Ethidium bromide
Fluorescence quenching
Bile acid
Global analysis

ABSTRACT

Photoluminescence behavior of ethidium bromide (EB) was studied in homogeneous solvents as well as in presence of bile acid surfactants. A quantitative analysis based on Kamlet–Taft equation toward the contribution of different solvatochromic parameters like solvent polarizability (π^*), hydrogen bond donor (α) and hydrogen bond acceptor (β) ability, on EB spectral properties reveals that though fluorescence quantum yield and lifetime do not show any straight forward correlation individually, the substantial decrease in these quantities is due to the increase in total nonradiative decay rate in polar protic medium. The interaction of EB with bile acid hosts gives rise to large increase in fluorescence intensity due to shielding of the probe in less hydrogen bonding environment. Global analysis of the fluorescence decay behavior indicates that more than 50% of the fluorophores get sequestered inside the micellar sub-domain with an apparent binding constant of $\sim 10^3\ M^{-1}$.

1. Introduction

Ethidium bromide (3,8-diamino-5-ethyl-6-phenyl phenanthridiniumbromide, EB) is a cationic dye and an antiviral drug that interacts strongly and specifically with both double stranded DNA and RNAs. They bind DNA and RNA via intercalative mode between adjacent base pairs and elongate of double helical structure [1–8]. Because of the appreciable change in fluorescence intensity upon binding, EB is widely used as fluorescence bio-marker. More than 10 fold increase in the emission intensity and decay time is observed when EB binds to DNA in comparison with the bulk water [9]. There are numerous studies on EB with polynucleotide; however, surprisingly, reports on the investigation of EB fluorescence enhancement upon binding with DNA as well as possibility to use it as fluorescence probe in microenvironments other than DNA are relatively scarce. To understand the solvent dependent photophysics and fluorescence intensity change in EB, Olmstead and Kearns [10] concluded that the amino proton of the ethidium ion becomes quite acidic in one of its quinoid structures (see Chart 1), even in the ground state, which further increases in the excited state so that EB donates one of the amino protons to the surrounding solvent environment. This excited state proton donation process is the most dominant relaxation pathway and responsible for the low fluorescence yield in polar/protic solvents. Based on these findings and further investigation, Pal et al. [11] recently suggested that the nonradiative pathway of EB strongly depends on the hydrogen bond accepting (HBA) basicity of the solvent rather than the polarity.

Research in the field of bile acids (BAs) has received considerable interest in recent times both from their biochemistry and physiology [12–14]. BAs are steroid acids found predominantly in the bile of mammals. Bile acids aid in fat absorption and modulate cholesterol levels. They are produced from cholesterol in the liver and are stored in the gall bladder. Gall bladder contraction with feeding releases bile acids into the intestine. Bile acids undergo enterohepatic circulation, i.e. they are absorbed in the intestine and taken up by hepatocytes for re-excretion into bile. Measurement of bile acid concentrations is, therefore, a good indicator of hepatobiliary function, but is not specific for the type of underlying diseases.

The most important bile acids in humans are cholic acid (CA), deoxycholic acid (DCA), and chenodeoxycholic acid (CDCA) (Scheme 1). All bile acids consist of two connecting units, a rigid steroid nucleus and a short aliphatic side chain [15]. The steroid nucleus of BAs has the saturated tetracyclic hydrocarbon perhydrocyclopentanophenanthrene, containing three six-member rings and a five member ring. The one or more α-oriented hydroxyl groups of BAs are put on the concave surface (α-face) of the steroid backbone and the methyl groups are positioned on the opposite convex side (β-face). Free molecules of BAs, normally cylindrical shapes of 20 Å long with a radius of about 3.5 Å, have a great surface activity and inclination to the formation of large aggregates, owing to the difference in orientation of hydrophilic and hydrophobic groups on the steroid ring systems.

* Corresponding author. Tel.: +91 364 2722634; fax: +91 364 2550076.
E-mail addresses: smitra@nehu.ac.in, sivaprasadm@yahoo.com (S. Mitra).

1010-6030/$ – see front matter © 2012 Elsevier B.V. All rights reserved.
http://dx.doi.org/10.1016/j.jphotochem.2012.06.019

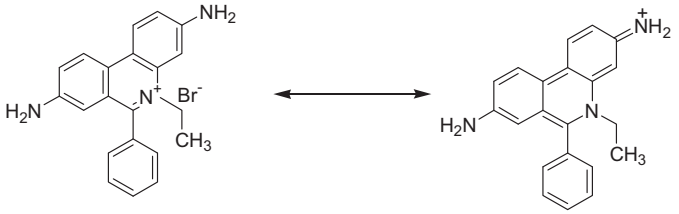

Chart 1. Structures of different resonance forms of ethidium bromide (EB).

In contrast to the spherical nature of the pseudo-particle formed due to the self aggregation of linear surfactant molecules like sodium dodecyl sulfate (SDS), cetyltrimethyl ammonium bromide (CTAB) and/or triton-X 100 (TX-100), the BAs consist of a rigid steroid backbone giving rise to the concave side with polar hydroxyl group (α-face) and the methyl groups in the convex side (β-face). Aggregation of BAs in aqueous solution is due to hydrophobic interaction of the apolar β-faces of steroid backbones with possibility of further aggregation through hydrogen bonding in the α-faces [16]. This unique arrangement based on facial amphiphilicity renders a different aggregation pattern in BAs (Scheme 1) unlike the conventional surfactants; where, the micellar structure is mostly approximated to be spherical originated from the mutual arrangement of the head and tail groups with different hydrophobicity [17–20]. Therefore, to study the interaction of EB with aggregated BA host seems interesting and can be approximated as a biological model to mimic the DNA intercalation process. In this work we report the results of detailed steady state and time-resolved study on the fluorescence behavior of EB in several homogeneous environments consisting of neat and mixed solvent systems, and also in presence of BAs like CA, DCA and CDCA.

Table 1
Solvent parameters.

No.	Solvent	$\Delta f(\varepsilon,n)$[a]	$E_T(30)$[b]	α[c]	β[c]	π^*[c]
1	1,4-Dioxane	0.03	36	0	0.37	0.55
2	Ethyl acetate	0.19	38.1	0	0.45	0.55
3	Terahydrofuran	0.21	37.4	0	0.55	0.58
4	Dichloromethane	0.22	40.7	0	0.1	0.81
5	1-Butanol	0.26	49.7	0.84	0.84	0.47
6	Dimethyl sulfoxide	0.26	45.1	0	0.76	0.1
7	Dimethyl formamide	0.27	43.2	0	0.69	0.88
8	1-Propanol	0.27	50.7	0.84	0.9	0.52
9	Isopropyl alcohol	0.27	48.4	0.76	0.95	0.48
10	Accetone	0.28	42.2	0.08	0.48	0.71
11	Acetonirile	0.3	45.6	0.19	0.4	0.75
12	Methyl alcohol	0.31	55.4	0.98	0.66	0.6
13	Water	0.32	63.1	1.17	0.47	1.09

[a] Polarity parameter $\left(=\frac{\varepsilon-1}{2\varepsilon+1}-\frac{n^2-1}{2n^2+1}\right)$ where, solvent dielectric constant and refractive indices are represented by ε and n, respectively.
[b] Reichardt solvent parameter.
[c] Kamlet–Taft solvent parameters.

2. Experimental

Analytical grade ethidium bromide (EB) was procured from Sisco Research Laboratories (SRL), India (product no. 054817) and the purity was checked by chromatographic techniques before use. The organic solvents used were of spectroscopic grade (>99.5%) as received from Alfa Aesar and, in some cases, from Aldrich Chemical Company. The solvents and the corresponding solvatochromic parameters are listed in Table 1. The bile acids viz. CA, DCA and CDCA were all obtained from Sigma–Aldrich Chemical Pvt. Ltd. (product no. C1129, D2510 and C9377, respectively) and used as received in freshly prepared aqueous buffer solution of pH = 9.2 by dissolving one buffer tablet obtained from Qualigens fine chemicals (a division of GlaxoSmithkline Pharmaceuticals Ltd.), India in

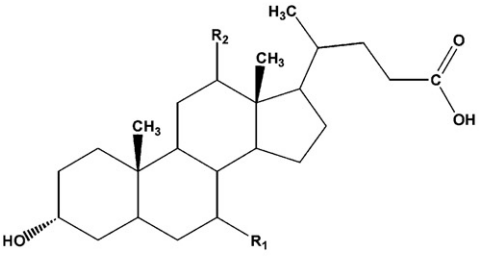

Bile acid (BA)	R_1	R_2
Cholic Acid (CA)	α-OH	α-OH
Deoxycholic acid (DCA)	H	α-OH
Chenodeoxycholic acid (CDCA)	α-OH	H

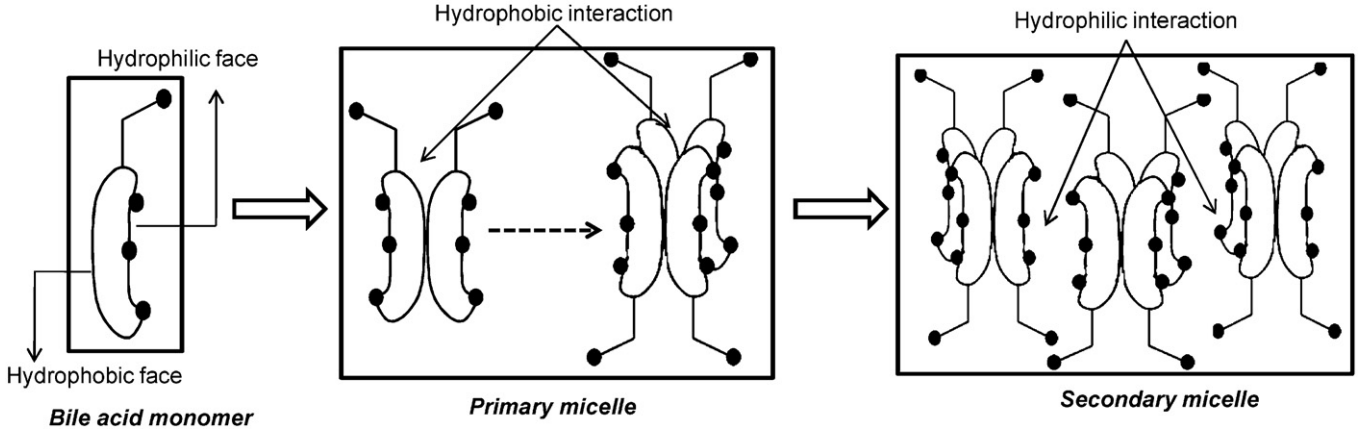

Scheme 1. Structures of different bile acid (BA) used in this study. The two step aggregation pattern of BA monomers adapted from reference [33] has also been demonstrated in the lower panel.

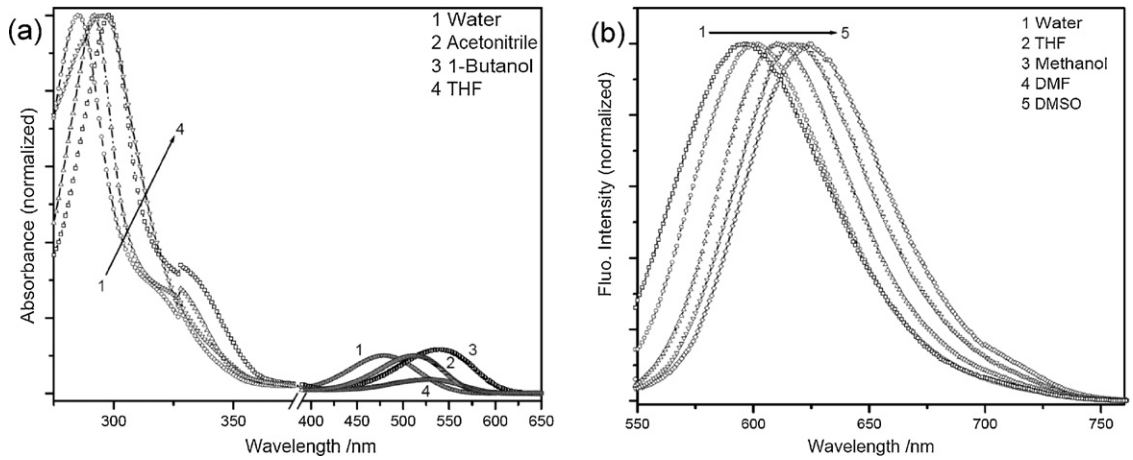

Fig. 1. Normalized absorption (a) and fluorescence emission (b) spectra of 6 μM EB solution in some selected solvents. The fluorescence emission was collected by exciting the sample in the low energy absorption region in each case.

100 ml water. The water used as solvent in all the measurements was obtained from Elix10 water purification system (Millipore India Pvt. Ltd.). All experiments were carried out at ambient temperature of 293 K. EB is sparingly soluble in some of the organic solvents studied here. In those cases, the working solution in the concentration range of about 5–10 μM was prepared by diluting a very small quantity of stock EB solution in acetone with excess amount of desired solvent (>95%, v/v) and subsequent removal of acetone with slow evaporation, wherever possible. The final concentration was estimated photometrically by checking the optical density at 480 nm (ε_{480} = 5860 cm^{-1} M^{-1}) [21]. It is already known that EB forms the dimer in solution at the concentration range of ~10^{-3} M and because of the very low value of the dimerization constant (~50 M^{-1} in aqueous medium at 293 K), the possibility of formation of higher aggregates is negligible [22,23]. The concentration range of EB used in this study is less by about three orders of magnitude and rules out the possibility of the presence of EB dimer and/or any higher order aggregates.

Steady-state absorption spectra were recorded on a Perkin-Elmer model Lambda25 absorption spectrophotometer. Corrected fluorescence spectra were taken in a Hitachi model FL4500 spectrofluorimeter. Quartz cuvettes of 10 mm optical path length received from PerkinElmer, USA (part no. B0831009) and Hellma, Germany (type 111-QS) were used for measuring absorption and fluorescence spectra, respectively. In both fluorescence emission and excitation spectra measurements, 5 nm bandpass was used in the excitation and emission side. Fluorescence quantum yields (ϕ_f) were calculated by comparing the total fluorescence intensity (F) under the whole fluorescence spectral range with that of quinine bisulfate in 0.5 M H_2SO_4 solution ($\phi_f^s = 0.546$ [24]), using the following equation.

$$\phi_f^i = \phi_f^s \cdot \frac{F^i}{F^s} \cdot \frac{1 - 10^{-A^s}}{1 - 10^{-A^i}} \cdot \left(\frac{n^i}{n^s}\right)^2 \quad (1)$$

where, A^i and A^s are the optical density of the sample and standard, respectively, and n^i is the refractive index of solvent at 293 K. The relative experimental error of the measured quantum yield was estimated within ±10%.

The fluorescence decay curves in homogeneous solvents as well as in presence of bile acids were obtained using LED based time correlated single photon counting (TCSPC) system obtained from Photon Technology International (PTI). The excitation was done at 525 nm. The instrument response function (IRF) was obtained by using a dilute colloidal suspension of dried non-dairy coffee whitener. The experimentally obtained fluorescence decay traces $I(t)$, collected at the magic angle (54.7°) to eliminate any contribution from the anisotropy decay, were expressed as a sum of exponentials (Eq. (2)) and analyzed by non–linear least–square iterative convolution method based on Lavenberg–Marquardt [25] algorithm as implemented in the data analysis software (FelixGX version 4.0) from PTI.

$$I(t) = \sum_i \alpha_i \exp\left(\frac{-t}{\tau_i}\right) \quad (2)$$

where, α_i is the amplitude of the ith component associated with fluorescence lifetime τ_i such that $\sum \alpha_i = 1$. The reliability of fitting was checked by numerical value of reduced chi-square (χ^2), Durbin–Watson (DW) parameter and also by visual inspection of residual distribution in the whole fitting range [26].

3. Results and discussion

3.1. Steady state and time-resolved fluorescence in homogeneous media

Fig. 1 depicts some representative absorption and emission profile of EB in homogeneous solvents; whereas, the spectral parameters are collected in Table 2. As noted earlier, EB shows an intense UV band along with one weaker charge transfer absorption at ~500 nm in all the solvents. Excitation at both the major absorption bands leads to emission at ca. 600 nm. The fluorescence decay time (τ_f) of EB in different solvents is also incorporated in Table 2. In most of the solvents EB fluorescence shows single exponential decay (Fig. 2a) and the calculated lifetimes are in good agreement with those reported earlier [10,11]. Slight difference in τ_f values is also noted from the data reported by Pal et al. [11] in some of the solvents. This might be due to the different excitation wavelength used to measure the fluorescence decay time. Nevertheless, the most important observation is that in some of the solvents mentioned in Table 2, two-exponential fitting is required for adequate reproduction of experimental data points as confirmed by better statistical parameters and also by visual inspection of the distribution of weighted residual/autocorrelation function etc. Some of the representative examples are shown in Fig. 2b as well as in the supplementary section (Fig. 1S). The appearance of the small fraction of second component with slower decay time, particularly in higher alcohols, might be considered as due to the solvated charged species (ethidium ion). Instead of giving too much importance to individual decay components, we define the amplitude weighted average decay time (given

Table 2
Fluorescence spectral properties of EB in homogeneous solvents.[a]

Solvent	Absorption maxima/nm	Emission maxima/nm	Stokes shift[b]/cm^{-1}	Fluo. yield[c]	Average lifetime[d]/ns
1	300, 544	625	2050.5	0.0061	–
2	297, 535	610	2298.1	0.0031	–
3	292, 528	600	2272.7	0.0666	10.5
4	292, 515	593	2554.1	0.2055	14.6
5	298, 539	621	2449.8	0.0961	5.9
6	300, 535	624	2665.9	0.0218	4.7
7	298, 533	618	2580.5	0.0327	5.2
8	298, 537	619	2466.9	0.0690	6.3
9	298, 541	615	2224.1	0.0753	-
10	297, 520	593	2367.4	0.0086	9.0
11	292, 513	597	2742.7	0.2293	9.2
12	294, 524	610	2690.5	0.0698	6.0
13	285, 480	599	4138.8	0.022	1.9

[a] The name of the solvents are listed in Table 1.
[b] Stokes shift ($\Delta\upsilon_{SS}$) calculated based on low-energy absorption band.
[c] Fluorescence quantum yield (ϕ_f), error limit ± 10%.
[d] Average fluorescence lifetime ($\langle\tau\rangle$) calculated from Eq. (3), error limit ±0.1 ns.

in Eq. (3)) of EB to discuss the fluorescence decay behavior. The calculated values are also listed in Table 2.

$$\langle\tau\rangle = \sum_i \alpha_i \times \tau_i \quad (3)$$

3.2. Solvatochromism in EB spectral properties

As with the ground state absorption bands, the relatively broad fluorescence emission band of EB is also sensitive to its microenvironment. However, apparently none of the spectral parameters show any significant degree of correlation with the solvent properties. Previously, the increase in EB fluorescence quantum yield (ϕ_f) and lifetime (τ_f) has been related to the solvent hydrogen bond accepting ability (HBA) [11]. However, the observations were restricted in few solvents only and a global picture of solvent effect was lacking. Furthermore, the solvent dependence of absorption and fluorescence spectral shift was not discussed at all. In this report we try to analyze variation in spectral position as well as intensity in terms of several solvent parameters. Interestingly, the Stokes shift shows almost similar correlation either with the polarity parameter $\Delta f(\varepsilon,n)$, calculated from the solvent dielectric constant (ε) and refractive indices (n) with the following relation:

$$\Delta f(\varepsilon, n) = \frac{\varepsilon - 1}{2\varepsilon + 1} - \frac{n^2 - 1}{2n^2 + 1} \quad (4)$$

or, with solvent polarity scale, $E_T(30)$. The resultant correlation diagrams are shown in the supplementary section (Fig. 2S). The uni-parametric empirical solvent polarity scale, $E_T(30)$, essentially depends on both the solvent dielectric properties and hydrogen bonding ability [27]. Therefore, the combined effect of solvent polarity and hydrogen bonding on spectroscopic parameters of EB were analyzed by means of the linear solvation energy relationship (LSER) concept using Kamlet–Taft relation given below (Eq. (5)) [28],

$$P = P^0 + s\pi^* + a\alpha + b\beta \quad (5)$$

where, P is the value of the solvent dependent property to be modeled, P^0, s, a and b are the coefficients determined from the LSER analysis. The term π^* indicates the measure of solvent dipolarity/polarizability [29], whereas, α and β is the scale of hydrogen bond donation acidity and acceptance basicity of the solvent, respectively [30]. The corresponding parameters for all the solvents are taken from literature [31,32] and the correlations were carried out by multiple linear regression analysis as implemented in ORIGIN 6.0 (Microcal Inc.) program package as discussed before [33,34]. Fig. 3a shows the correlation diagram for the Stokes shift and the correlation equation is given below. It is readily seen that the maximum contribution (ca. 40%) in EB Stokes shift is due to solvent π^*. This strong correlation can be explained by the fact that both the absorption and fluorescence emission maxima of charged EB are strongly modulated by solvent dielectric properties, as indeed

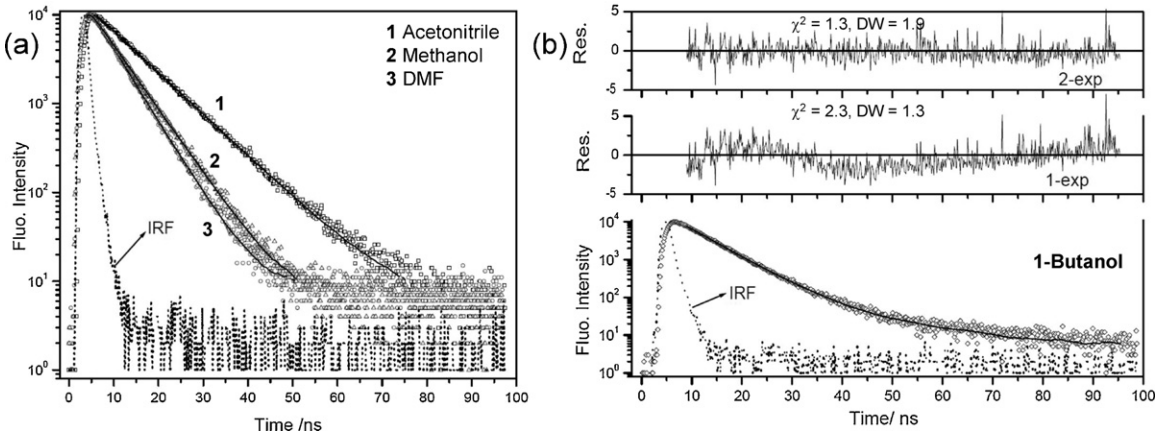

Fig. 2. Time-resolved fluorescence decay traces (open circle) of 6 μM EB solution in some of the selected solvents along with the fitting data (solid line) and instrument response function (IRF) for single exponential case (a) and two exponential case (b). The requirement of two exponential fitting in (b) is confirmed by comparing the distribution of weighted residuals and other statistical parameters.

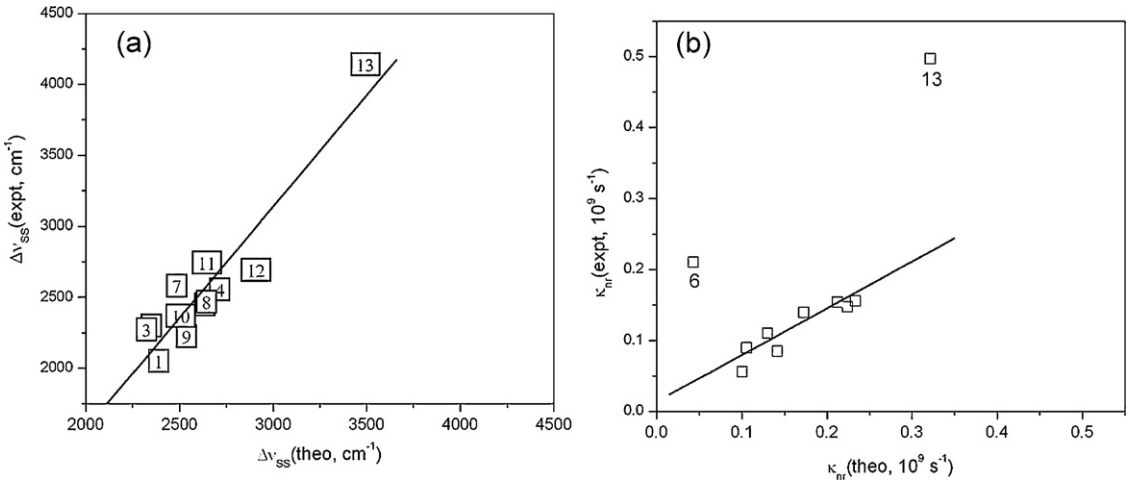

Fig. 3. Correlation diagram of EB Stokes shift ($\Delta\upsilon_{SS}$) (a) and total nonradiative decay rate (κ_{nr}) (b) with theoretically predicted values obtained multiple regression method using Kamlet–Taft equation.

mentioned before.

$$\nu_{SS}(\text{cm}^{-1}) = 2150.04 + 636.70 \times \alpha - 483.48 \times \beta + 759.13 \times \pi^* \quad (6a)$$

$$\kappa_{nr}(10^9, \quad \text{s}^{-1}) = -0.0498 + 0.116 \times \alpha + 0.0997 \times \beta + 0.1732 \times \pi^* \quad (6b)$$

However, neither fluorescence quantum yield (ϕ_f) nor the decay time (τ) shows any correlation with the solvent properties. Instead, the total nonradiative decay parameter, $\kappa_{nr} = (1 - \phi_f)/\tau_f$, shows reasonably good correlation (Fig. 3b) with the relationship indicated in Eq. (6b). Again, contribution from π^* is the maximum; and interestingly, increase in values of solvent parameters lead to the increase in total nonradiative rate, which essentially implies the lowering in the value of either ϕ_f or τ_f or both. This observation is consistent with earlier reports [10,11] and can explain very low values of ϕ_f and τ_f of EB in water and/or polar protic solvents in comparison with other organic solvents. Interestingly, the spectral parameters of bulk water solution never correlate with other solvents indicating a different and more complicated deactivation mechanism. Similar observation has also been reported earlier for EB solvatochromism. Also, it is seen in Fig. 3(b) that the κ_{nr} value in case of DMSO is not correlated at all with other solvents. It is to be noted here that DMSO is a strongly basic solvent with high β value; however, both the α as well as π^* values are extremely low (Table 1). This further indicates that solvatochromism in EB is not controlled by solvent basicity (β) only, other parameters like α and π^* also play crucial role. Recently we have shown that the excited state photophysics of strongly fluorescent luminol molecule is mainly controlled by solvent acidity (α) only [33]; however, for a biologically important flavin like 7,8-dimethylalloxazine with almost similar structure to luminol, both solvent π^* and α contribute almost equally in the excited state photophysics [34]. On the other hand, the fluorescence spectral properties of an intramolecular charge transfer (ICT) probe like *trans*-ethyl *p*-(dimethylamino) cinnamate is exclusively controlled by solvent π^* parameter only [35]. Obviously, it is not possible to make any general statement on the variation of spectroscopic behavior of fluorescent molecules with solvent parameters; though careful analysis certainly reveals the nature of excited state for a particular system. In case of EB, interaction with the solvent might drastically change the relative ordering of the excited state energy levels. With increasing π^* and α (for example in water) both the fluorescence yield (ϕ_f) and lifetime (τ_f) decreases to a considerable extent resulting an increase in total nonradiative rate constant (κ_{nr}).

3.3. Steady state and time-resolved fluorescence behavior of EB in mixed solvents

To study the influence of solvent on the excited state photophysical properties of EB, both steady state and time-resolved fluorescence of EB were studied in three homogeneous solvent mixtures, viz. acetonitrile/water, methanol/water and acetonitrile/DMSO. Addition of water in neat solution of EB either in acetonitrile or methanol decreases the fluorescence intensity gradually without any substantial change in the spectral position (Fig. 4); more particularly for the acetonitrile/water system. The fluorescence quenching data follow simple Stern–Volmer (S–V) relationship till ~80% (v/v) water content in acetonitrile before undergoing an upward deviation. Similar observation was also made for EB/methyl alcohol solution at about ~65% (v/v) water content. The S–V quenching constant was calculated from the linear segment of the data points and found to be about $(9.0 \pm 0.4) \times 10^6\ \text{M}^{-1}\ \text{s}^{-1}$ in both the cases. The deviation at high water content can be understood easily by considering a different solvation of the excited EB ion, as indeed observed in the previous section and also mentioned earlier [11]. However, the quenching of EB/acetonitrile solution in presence of DMSO is entirely different. Addition of even ~20% (v/v) DMSO causes the fluorescence red-shift of ~18 nm along with four fold decrease in fluorescence intensity. This observation is further confirmed from the steady state data of EB in pure solvents (Table 2). From the data of EB fluorescence maximum in different solvents, it is clear that the shift in acetonitrile/water and methanol/water mixed solvents vary within the range 2–10 nm; however, for acetonitrile/DMSO system it is more than 25 nm. Also, the fluorescence lifetime decreases to about 4.3 ns even in presence of ~20% (v/v) DMSO from 9.2 ns in pure acetonitrile. S–V analysis in this case shows a downward curvature; however, fluorescence lifetime remains more or less constant with further increase in DMSO content (Fig. 5). With all these notable differences, it can be concluded that the quenching of EB fluorescence in presence of DMSO follows a different type of interaction compared with water, which is induced probably due to very strong basic nature of DMSO.

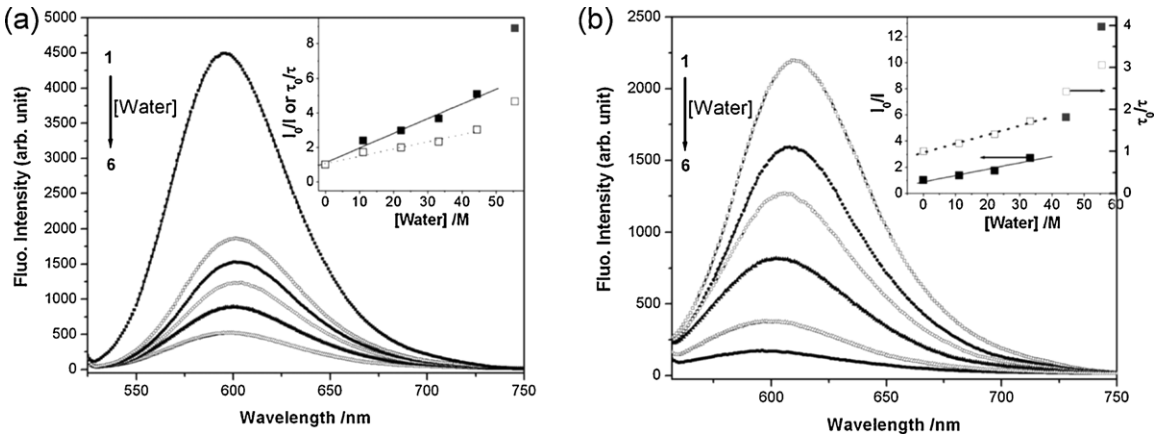

Fig. 4. Water assisted fluorescence quenching of EB in acetonitrile (a) and methyl alcohol (b). Volume % of water = 0(1), 20 (2), 40 (3), 60 (4), 80 (5) and 100 (6). [EB]/μM = 6 and 9 for (a) and (b), respectively. Inset shows the Stern–Volmer analysis of quenching data based on intensity (filled square) and lifetime (empty square).

3.4. Fluorescence enhancement of EB in presence of bile acid hosts

To study the influence of the medium on excited state photophysical properties of EB, fluorescence titration experiment of EB was done in presence of several bile acids (BAs) like CA, DCA and CDCA in aqueous buffer of pH 9.2. Although EB fluorescence maximum position and yield remain unchanged at this pH, fluorescence decay time was measured to be 1.6 ns in contrast to the corresponding value of 1.9 ns in neat water solution (the pH of which was independently measured to be 6.1) described in previous sections. On gradual addition of BA, the absorption spectral profile is affected only marginally even in presence of highest concentration of BA. The little increase in optical density of EB in presence of BAs is due to greater solubilization of the probe in water in presence of micellar environment. Slight red shift in absorption peak position of EB is also observed (Fig. 6a). Similar behavior was observed in the excitation spectra also. However, gradual addition of BAs is associated with a slight red shift in the emission maximum along with appreciable increase in fluorescence intensity in all the cases (Fig. 6b–d) indicating a strong excited state interaction of EB with BAs. Interestingly, while EB fluorescence maximum is red shifted by about 5 nm in both the cases of DCA and CDCA in comparison with that in aqueous buffer solution of pH 9.2, no detectable shift is observed in the case of CA. In analogy with the DNA intercalation mechanism, the fluorescence enhancement of EB in presence of BAs can also be assumed due to the binding of the probe in the micellar sub-domain. The red-shift in fluorescence emission maximum in the presence of DCA and CDCA is indicative of a strong interaction of EB with these micelles in comparison the CA.

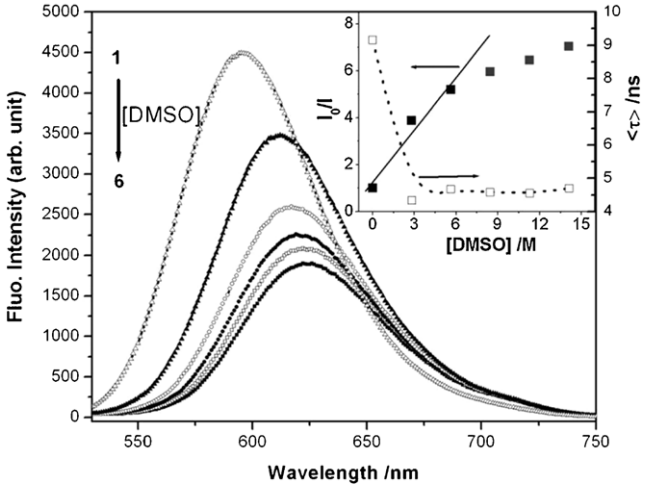

Fig. 5. Fluorescence quenching of EB/acetonitrile solution in presence of DMSO. [EB] = 6 μM and volume % of DMSO = 0(1), 20 (2), 40 (3), 60 (4), 80 (5) and 100 (6). Note that the data for the solutions from 2 to 6 were increased three times to make a legible presentation along with 1. Inset shows the Stern–Volmer analysis of quenching data based on intensity (filled square). The variation of EB fluorescence lifetime (empty square) with increase in DMSO concentration is also shown.

The striking feature of BA aggregation is that it is characterized by at least two cmc values. According to the primary–secondary micelle model of Small [36], at low concentrations, the BAs form small primary micelles with a characteristic cmc value. In this micelle, the BAs turn toward each other by their hydrophobic β-face. At the concentration range beyond second cmc, these primary micelles attach together to form large secondary micelles by hydrogen bonding interactions through their hydrophilic outer surface, resembling the internal hydrogen bonding pattern in DNA base pairs. A cartoon diagram of this aggregation pattern is shown in lower panel of Scheme 1. Also, in one of the relatively recent report by Lee et al. [37], it was shown that the interior polarity of the micro-aggregates formed from DCA modified chitosan is substantially reduced when compared with bulk water. Overall, it can be envisaged that, on binding with the BAs, EB is partially shielded both from dipolar and hydrogen bonding interaction originated from the solvent surroundings. Naturally, this leads to a decrease in total nonradiative rate (Eq. (6b)) and therefore, the fluorescence intensity increases substantially.

It is known that for the formation of primary micelle in BAs, the aggregation number is very small and it shows rather weak dependence on the surfactant concentration. The maximum surfactant concentration, for all the BAs used in this study, is always within 20 mM range and the aggregation number for the primary micelle formation can be assumed to be constant. With this approximation, qualitative estimation of the binding constant (K_S) values of EB with different BAs can be made within the model proposed by Hirose and Sepŭlveda [38] and successfully applied to a number of systems earlier [19,20] using the following equation.

$$\frac{F - F_0}{F_m - F_0} = K_S \times [D_t] \tag{7}$$

where, F, F_0, and F_m are the area under the whole fluorescence emission spectra of the probe in the surfactant, buffer solution and in fully micellized conditions, respectively. $[D_t]$ is the total surfactant concentration.

A plot of $(F-F_0)/(F_m-F_0)$ vs. $[D_t]$ gives a straight line, the slope of which gives the value of the binding constant, K_S. The corresponding values for CA, DCA and CDCA were found to be $(0.63 \pm 0.12) \times 10^3\ M^{-1}$, $(2.04 \pm 0.50) \times 10^3\ M^{-1}$ and

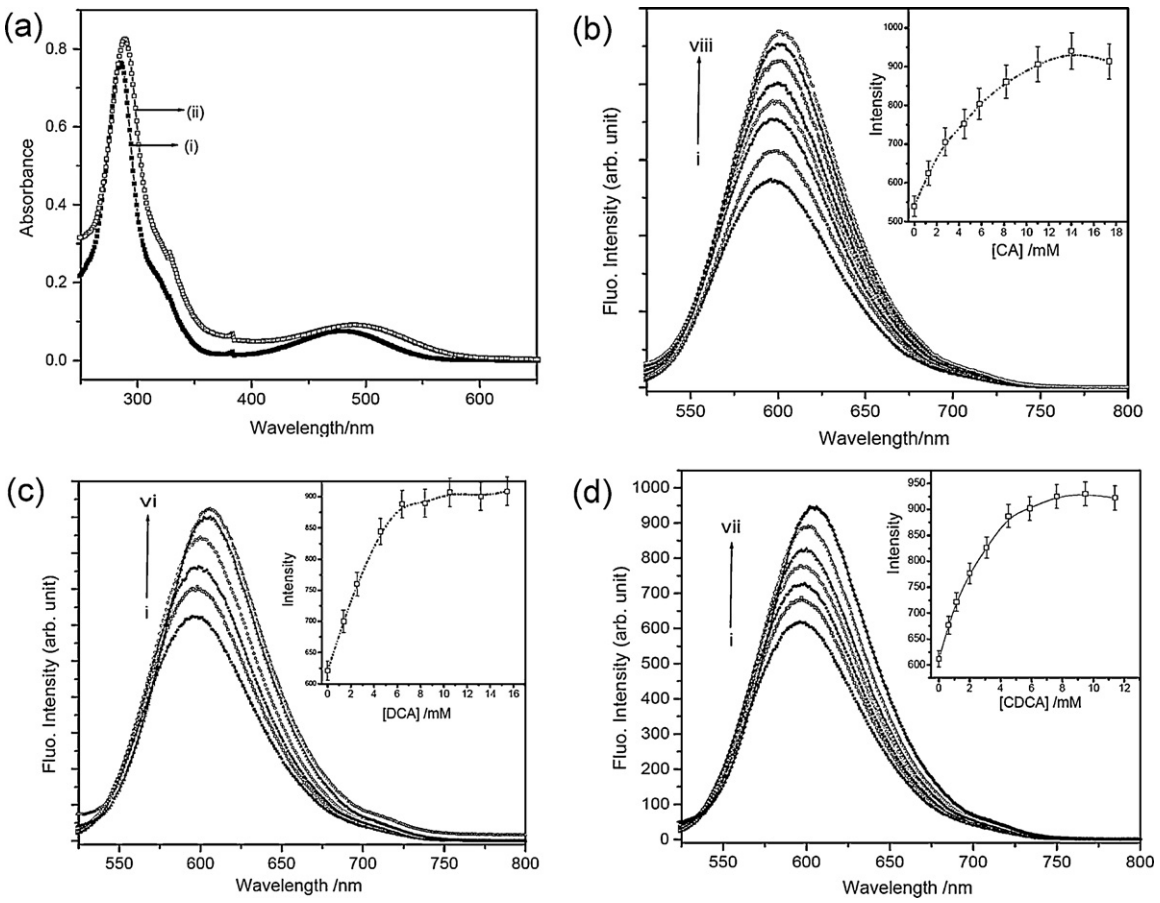

Fig. 6. (a) Absorption spectra of EB solution in aqueous buffer of pH = 9.2 (i) and in presence of 14 mM CA (ii); (b–d) Enhancement of EB fluorescence emission with gradual addition of BAs. [EB] = ~10 μM in each case. Inset shows the variation in fluorescence intensity at 597 nm with BA concentration.

$(2.20 \pm 0.34) \times 10^3\ M^{-1}$, respectively which clearly indicates that the binding of EB is ca. 3–4 times stronger in DCA and CDCA in comparison with CA as indeed predicted earlier from fluorescence spectral shift. The data indicate that the replacement of hydroxy groups from the steroid ring increases the affinity of BA for EB. It is indeed well known that in vitro binding of BAs to exogenous substrates depends on the specific binding nature [39] and, therefore, the binding constant values in different cases may vary over huge range depending on the substrate as well as the receptor. Nevertheless, the binding constant values measured from the fluorescence based study on the interaction of BAs with human serum albumin (10^3–$10^4\ M^{-1}$) [40] is in good agreement with the values calculated from the present study. Interestingly, the binding constants of EB with the BAs calculated here is almost an order of magnitude higher than the corresponding values for an organic charge transfer system reported earlier [20]. On the other hand, EB binding to DNA base pairs as well as to different generation starburst dendritic structures occur with moderate binding affinity (10^4–$10^6\ M^{-1}$) [5,41]. The higher magnitude of EB binding to BAs indicates a favorable mode of intercalating interaction possibly due to different aggregation pattern in biological surfactants.

3.5. Fluorescence decay behavior of EB in presence of bile acid hosts

Excited state lifetime of a fluorophore in a micellar solution serves as a sensitive parameter for exploring the local environment and sequestration of fluorophore in micro-heterogeneous media. It also contributes to the understanding of different interactions between the probe and the micellar sub-domains [42]. On the basis of this time-resolved fluorescence was monitored for EB with each addition of different concentration of BAs. As mentioned earlier, the aqueous buffer (pH 9.2) solution of EB undergoes single exponential decay with a fluorescence lifetime of 1.6 ns. However, in micellar solutions, the decay curves show significant contributions from more than one component as evidenced by the visual inspection of distribution of weighted residuals as well as the reduced χ^2 values (Fig. 7) in presence of all the BAs studied here. Global analysis of all the decay functions at varying concentration of individual BA results an additional decay component of 4.6 ± 0.1 ns along with the $\sim 1.7 \pm 0.1$ ns component. In analogy with the previous discussion, the short lifetime component is essentially the fraction of total EB concentration remaining in the aqueous phase; whereas, the long component is due to the sequestered fluorophore bound in the micellar sub-domain.

Analysis of the variation of component contribution toward the total fluorescence decay indicates that the contribution of micelle bound EB having slower fluorescence decay time increases as we go on increasing the concentration of BA in the solution. This is quite obvious, as it is expected that the fraction of sequestered fluorophore will increase with increase in BA concentration. Interestingly, the ratio of the two component contribution, when plotted against BA concentration, shows a sharp break point in all the cases within 6.8 ± 0.3 mM concentration (Fig. 7, inset). As discussed above, the concentration range of BAs used in the present study only deals with the formation of primary micellar structure; therefore, this break point and the corresponding concentration can apparently be approximated as an indicator of

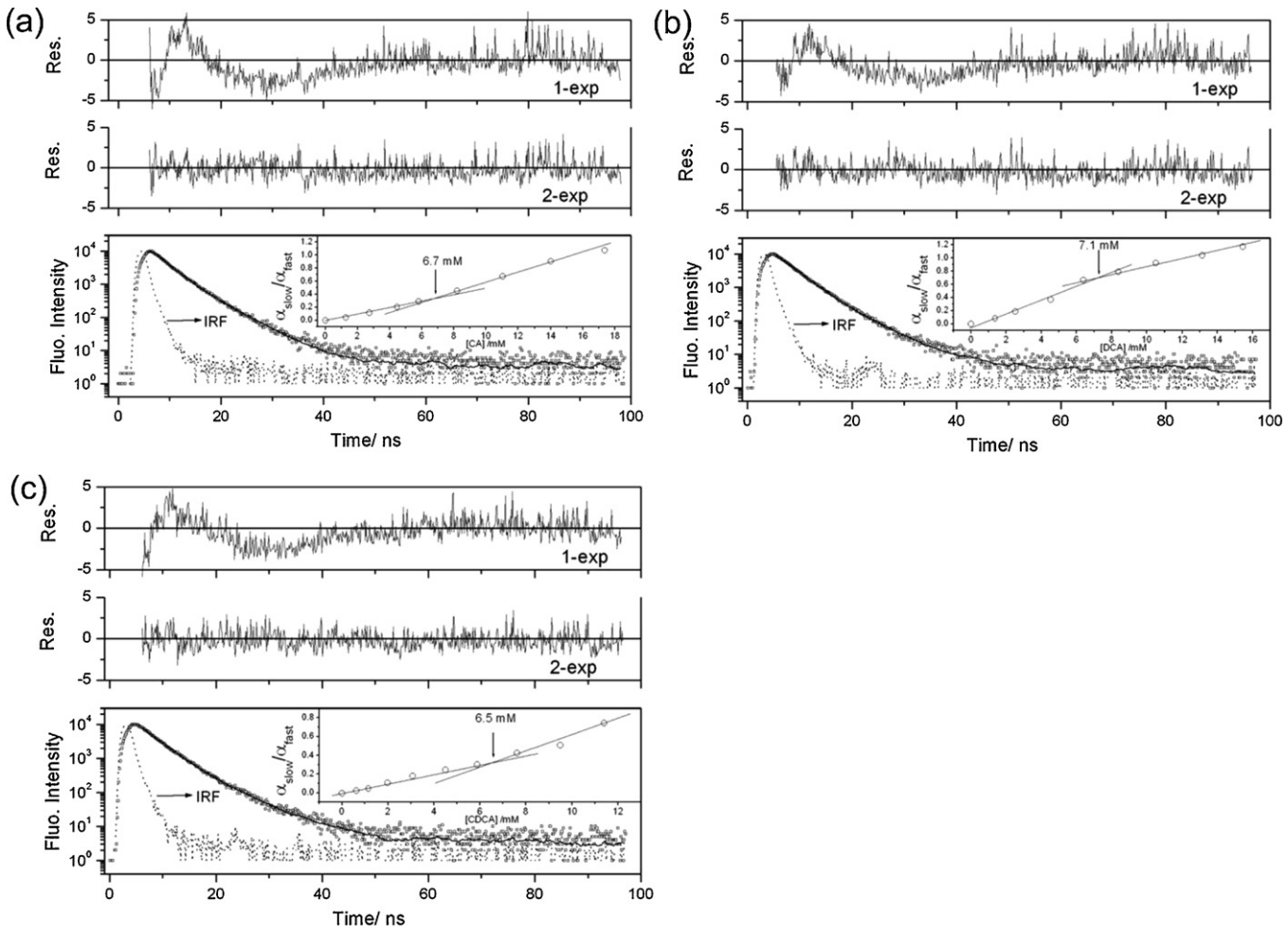

Fig. 7. Time-resolved fluorescence decay traces (open circle) of ~10 μM EB in buffer solution of pH = 9.2 in presence of CA (a), DCA (b) and CDCA (c) along with the simulated data (solid line) and instrument response function (IRF) for two exponential fitting. The concentration of bile acids was ~11.2 mM in all the cases. The upper panels show the distribution of weighted residuals in one and two exponential fitting, respectively.

critical micelle concentration (cmc). The estimated cmc values are in good agreement with the data available in the literature [43].

4. Conclusions

The detailed fluorescence behavior and solvatochromism of ethidium bromide (EB) was studied in neat and mixed homogeneous solvents as well as in presence of natural surfactants like bile acid by steady state and time-resolved fluorescence spectroscopy. The observed solvatochromism and increase in fluorescence intensity of EB in polar aprotic media is rationalized by multi-parametric approach using Kamlet–Taft equation. It has been found that the total nonradiative decay rate is strongly correlated with solvent properties and explains the dramatic decrease in either fluorescence yield or lifetime of EB in polar protic environment. Water assisted EB fluorescence quenching either in acetonitrile or methanol follows simple Stern–Volmer (SV) mechanism; however, strongly basic solvent DMSO quenches the fluorescence in an entirely different mechanism. All the BAs bind EB with moderate affinity and causes significant increase in fluorescence intensity by shielding the fluorophore from relatively more polar and hydrogen bonding aqueous phase. The heterogeneous distribution of fluorophore in micellar sub-domain is evident from additional slower fluorescence decay component. The sharp break point observed in the population ratio of long to short decay component can efficiently monitor the onset of primary aggregation pattern in BA micelles.

Acknowledgement

Financial support through research project 2009/37/26 from the Board of Research in Nuclear Sciences (BRNS), Government of India is gratefully acknowledged. Thanks are also due to UGC and DST for supporting the Department of Chemistry through DSA-SAP and FIST, respectively.

Appendix A. Supplementary data

Supplementary data associated with this article can be found, in the online version, at http://dx.doi.org/10.1016/j.jphotochem.2012.06.019.

References

[1] D. Pastré, O. Piétrement, A. Zozime, E. Le Cam, Study of the DNA/ethidium bromide interactions on mica surface by atomic force microscope: influence of the surface friction, Biopolymers 77 (2005) 53–62.
[2] M.R. Bugs, M.L. Cornélio, Analysis of the ethidium bromide bound to DNA by photoacoustic and FTIR spectroscopy, Photochemistry and Photobiology 74 (2001) 512–520.
[3] N.W. Luedtke, Q. Liu, Y. Tor, On the electronic structure of ethidium, Chemistry: A European Journal 11 (2004) 495–508.

[4] M.J. Waring, Complex formation between ethidium bromide and nucleic acids, Journal of Molecular Biology 13 (1965) 269–282.
[5] J.-B. Lepecq, C. Paoletti, A fluorescent complex between ethidium bromide and nucleic acids: physical–chemical characterization, Journal of Molecular Biology 27 (1967) 87–106.
[6] R.J. Douthart, J.P. Burnett, F.W. Beasley, B.H. Frank, Binding of ethidium bromide to double-stranded ribonucleic acid, Biochemistry 12 (1973) 214–220.
[7] C.-C. Tsai, S.C. Jain, H.M. Sobell, Visualization of drug-nucleic acid interactions at atomic resolution: I. Structure of an ethidium/dinucleoside monophosphate crystalline complex, ethidium: 5-iodouridylyl (3′–5′) adenosine, Journal of Molecular Biology 114 (1977) 301–315.
[8] S. Nafisi, A.A. Saboury, N. Keramat, J.-F. Neault, H.-A. Tajmir-Riahi, Stability and structural features of DNA intercalation with ethidium bromide, acridine orange and methylene blue, Journal of Molecular Structure 827 (2007) 35–43.
[9] D.P. Heller, C.L. Greenstock, Fluorescence lifetime analysis of DNA intercalated ethidium bromide and quenching by free dye, Biophysical Chemistry 50 (1994) 305–312.
[10] J. Olmsted III, D.R. Kearns, Mechanism of ethidium bromide fluorescence enhancement on binding to nucleic acids, Biochemistry 16 (1977) 3647–3654.
[11] S.K. Pal, D. Mandal, K. Bhattacharyya, Photophysical processes of ethidium bromide in micelles and reverse micelles, Journal of Physical Chemistry B 102 (1998) 11017–11023.
[12] A.F. Hofmann, in: T. Northfield, P.L. Zentler-Munro, R.P. Jazrawi (Eds.), Bile Acids and Hepatobiliary Disease, Kluwer, Boston, 1999, pp. 303–332.
[13] P.P. Nair, D. Kritchevsky, in: P.P. Nair, D. Kritchevsky (Eds.), The Bile Acids: Chemistry, Physiology and Metabolism, vol. 1, Plenum Press, New York, 1971, pp. 1–9.
[14] D.J. Parks, S.G. Blanchard, R.K. Bledsoe, G. Chandra, T.G. Consler, S.A. Kliewer, J.B. Stimmel, T.M. Willson, A.M. Zavacki, D.D. Moore, J.M. Lehmann, Bile acids: natural ligand for an orphan nuclear receptor, Science 284 (1999) 1365–1368.
[15] A.F. Hofmann, In the Liver: Biology and Pathology, 3rd ed., Raven Press, New York, 1994, p677.
[16] S. Mukhopadhyay, U. Maitra, Chemistry and biology of bile acids, Current Science 87 (2004) 1666–1683.
[17] V. De Giorgio, M. Conti (Eds.), Physics of Amphiphiles, Micelles, Vesicles and Microemulsions, North-Holland, Amsterdam, 1985.
[18] T.S. Singh, S. Mitra, Fluorescence behavior of intramolecular charge transfer probe in anionic, cationic, and nonionic micelles, Journal of Colloid and Interface Science 311 (2007) 128–134.
[19] T.S. Singh, S. Mitra, Fluorimetric studies on the binding of 4-(dimethylamino)cinnamic acid with micelles and bovine serum albumin, Photochemical and Photobiological Sciences 7 (2008) 1063–1070.
[20] T.S. Singh, S. Mitra, Fluorescence properties of *trans*-ethyl-*p*-(dimethylamino) cinnamate in presence of bile acid host, Journal of Photochemistry and Photobiology Part B: Biology 96 (2009) 193–200.
[21] M. Collini, L. D'Alfonso, G. Baldini, Trehalose-induced changes of the ethidium hydration shell detected by time-resolved fluorescence, Photochemistry and Photobiology 77 (2003) 376–382.
[22] M. Guenza, C. Cuniberti, The ethidium bromide dimer. Absorption and fluorescence properties in aqueous solutions, Spectrochimica Acta. Part A, Molecular and Biomolecular Spectroscopy 44 (1988) 1359–1364.
[23] B. Gaugain, J. Barbet, R. Oberlin, B.P. Roques, J.-B. Le Pecq, DNA bifunctional intercalators. 1. Synthesis and conformational properties of an ethidium homodimer and of an acridine ethidium heterodimer, Biochemistry 17 (1978) 5071–5078.
[24] S.R. Meech, D. Phillips, Photophysics of some common fluorescence standards, Journal of Photochemistry 23 (1983) 193–217.
[25] P.R. Bevington, Data Reduction and Error Analysis for the Physical Sciences, McGraw-Hill, New-York, 1969.
[26] J.R. Lakowicz, Principles of Fluorescence Spectroscopy, 3rd ed., Springer, Singapore, 2006 (Chapter 4).
[27] C. Reichardt, Solvatochromic dyes as solvent polarity indicators, Chemical Reviews 94 (1994) 2319–2358.
[28] M.J. Kamlet, J.M. Abboud, R.W. Taft, An examination of linear solvation energy relationships, Progress in Physical Organic Chemistry 13 (1981) 485–630.
[29] J.L. Abboud, M.J. Kamlet, R.W. Taft, Regarding a generalized scale of solvent polarities, Journal of the American Chemical Society 99 (1977) 8325–8327.
[30] J.V. Miller, E.G. Bartick, Forensic analysis of single fibers by Raman spectroscopy, Applied Spectroscopy 55 (2001) 1729–1732.
[31] Y. Marcus, The properties of organic liquids that are relevant to their use as solvating solvents, Chemical Society Reviews 22 (1993) 409–416.
[32] M.J. Kamlet, J.L.M. Abboud, M.H. Abraham, R.W. Taft, Linear solvation energy relationships. 23. A comprehensive collection of the solvatochromic parameters π^*, α, and β, and some methods for simplifying the generalized solvatochromic equation, Journal of Organic Chemistry 48 (1983) 2877–2887.
[33] N.S. Moyon, A.K. Chandra, S. Mitra, Effect of solvent hydrogen bonding on excited-state properties of luminol: a combined fluorescence and DFT study, Journal of Physical Chemistry A 114 (2010) 60–67.
[34] N.S. Moyon, S. Mitra, Fluorescence solvatochromism in lumichrome and excited-state tautomerization: a combined experimental and DFT study, Journal of Physical Chemistry A 115 (2011) 2456–2464.
[35] T.S. Singh, N.S. Moyon, S. Mitra, Effect of solvent hydrogen bonding on the photophysical properties of intramolecular charge transfer probe *trans*-ethyl *p*-(dimethylamino) cinamate and its derivative, Spectrochimica Acta. Part A, Molecular and Biomolecular Spectroscopy 73 (2009) 630–636.
[36] D.M. Small, The physical chemistry of cholanic acids, in: P.P. Nair, D. Kritchevsky (Eds.), The Bile Acids: Chemistry, Physiology and Metabolism, vol. 1, Plenum Press, New York, 1971 (Chapter 8).
[37] K.Y. Lee, W.H. Jo, I.C. Kwon, Y.-H. Kim, S.Y. Jeong, Structural determination and interior polarity of self-aggregates prepared from deoxycholic acid-modified chitosan in water, Macromolecules 31 (1998) 378–383.
[38] C. Hirose, L. Sepŭlveda, Transfer free energies of p-alkyl-substituted benzene derivatives, benzene, and toluene from water to cationic and anionic micelles and to n-heptane, Journal of Physical Chemistry 85 (1981) 3689–3694.
[39] L. Accatino, F.R. Simon, Identification and characterization of a bile acid receptor in isolated liver surface membranes, Journal of Clinical Investigation 57 (1976) 496–508.
[40] A. Roda, G. Cappelleri, R. Aldini, E. Roda, L. Barbara, Quantitative aspects of the interaction of bile acids with human serum albumin, Journal of Lipid Research 23 (1982) 490–495.
[41] W. Chen, N.J. Turro, D.A. Tomalia, Using ethidium bromide to probe the interactions between DNA and dendrimers, Langmuir 16 (2000) 15–19.
[42] A. Maciejewski, J. Kubicki, K. Dobek, The origin of time-resolved emission spectra (TRES) changes of 4-aminophthalimide (4-AP) in SDS micelles. The role of the hydrogen bond between 4-AP and water present in micelles, Journal of Physical Chemistry B 107 (2003) 13986–13999.
[43] B.R. Simonović, M. Momirović, Determination of critical micelle concentration of bile acid salts by micro-calorimetric titration, Mikrochimica Acta 127 (1997) 101–104.